



# Cine and Multicontrast Late Enhanced MRI Registration for 3D Heart Model Construction

Fumin Guo<sup>1,2(✉)</sup>, Mengyuan Li<sup>3</sup>, Matthew Ng<sup>1,2</sup>, Graham Wright<sup>1,2</sup>,  
and Mihaela Pop<sup>1,2</sup>

<sup>1</sup> Sunnybrook Research Institute, University of Toronto, Toronto, Canada  
fumin.guo@sri.utoronto.ca

<sup>2</sup> Department of Medical Biophysics, University of Toronto, Toronto, Canada

<sup>3</sup> Department of Biomedical Engineering, University of Toronto, Toronto, Canada

**Abstract.** Cardiac MR imaging using multicontrast late enhancement (MCLE) acquisition provides a way to identify myocardium infarct scar and arrhythmia foci in the peri-infarct. In image-guided RF ablations of ventricular arrhythmia and computational modeling of cardiac function, construction of a 3D heart model is required but this is hampered by the challenges in myocardium segmentation and slice misalignment in MCLE images. Here we developed an approach for cine and MCLE registration, and MCLE scar-cine myocardium label fusion to build high-fidelity 3D heart models. MCLE-cine image alignment was initialized using a block-matching-based rigid registration approach followed by a deformable registration refinement step. The deformable registration approach employed a self similarity context descriptor for image similarity measurements, optical flow as a transformation model and convex optimization to derive the optimal solution. We applied the developed approach to a preclinical dataset of 10 pigs with myocardium infarction and evaluated the registration accuracy by comparing cine and MCLE myocardium masks using Dice-similarity-coefficient (DSC) and average symmetric surface distance (ASSD). For 10 pigs, we achieved a mean DSC of  $80.4 \pm 7.8\%$  and ASSD of  $1.28 \pm 0.47$  mm for myocardium with a mean runtime of 1.5 min for each dataset. These results suggest that the developed approach provide the registration accuracy and computational efficiency that may be suitable for clinical applications of cardiac MRI that involve a cine and MCLE MRI registration component.

**Keywords:** Multicontrast late enhancement MRI ·  
Myocardium infarct tissue characterization · Image registration ·  
Convex optimization

## 1 Introduction

Ventricular arrhythmia associated with myocardial infarction is a leading cause of death. Currently, arrhythmogenic foci are identified using surfacic and invasive electrophysiological mapping. Cardiac MRI using contrast-enhanced acquisitions, e.g., late gadolinium enhancement (LGE), provides a way to non-invasively

identify the arrhythmogenic foci hidden deep in the myocardium. In image-guided RF ablations of ventricular arrhythmogenic foci and computational modeling of cardiac function, construction of a 3D heart model that depicts the extent, location and transmural extent of myocardial infarct within the myocardium is urgently required. However, this is challenging because of the difficulties in myocardium segmentation and slice misalignment in late enhancement MR images. Cardiac MRI using cine acquisitions provide excellent visualization of myocardium and cine-myocardium may be employed to facilitate a 3D heart model construction but this requires cine-LGE MRI registration as a first step.

Limited efforts have been dedicated to cine-LGE MRI registration and most of these efforts aimed to propagate cine myocardium contours to LGE images for myocardium infarct scar heterogeneity characterization. For example, Chenoune et al. [2] initialized 3D cine and LGE MR alignment using image orientation and position information, and the rough alignments were refined using a rigid registration approach that employed normalized mutual information metrics and a Powell's optimization scheme. Wei et al. [12] registered cine to LGE images using an enhanced cross correlation-based constrained affine registration algorithm followed by a B-spline free-form deformable registration using pattern intensity. Tao et al. [11] performed global affine registration using Elastix toolbox and then locally refined cine-LGE alignments by maximizing the correlation between cine contour maps and LGE images.

Multicontrast late enhancement (MCLE) MRI represents a new method that also permits myocardium infarct tissue characterization and has demonstrated advantages over conventional LGE MRI [3]. Previous studies have shown that MCLE provides better SNR, higher contrast for improved myocardium infarct visualization and scar characterization. However, there are still known issues associated with myocardium segmentation and slice misalignment that hamper 3D MCLE-based heart model construction. In this work, we provided an approach for cine and MCLE cardiac MRI registration and cine myocardium-MCLE scar label fusion for 3D heart model construction. As shown in Fig. 1, our developed approach employed a rigid registration step to initialize the cine-MCLE alignment followed by a deformable registration component to refine the registration results. The resulting deformation field was used to transform MCLE-scar and cine-myocardium masks for label fusion and 3D heart model construction.

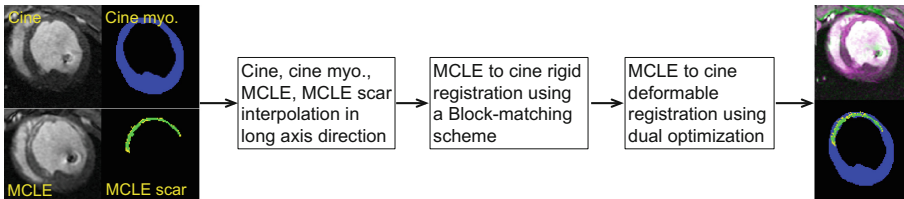


**Fig. 1.** Cine-MCLE registration and cine myocardium-MCLE scar fusion workflow.

## 2 Methods

### 2.1 Cine-MCLE Rigid Registration: A Block Matching Scheme

Rigid or affine registrations are usually performed to initialize the rough alignment of images prior to finer deformable registrations. Most of the rigid and affine registration methods involve finding a global relationship or correspondence of the features (i.e., image signal intensities, landmarks) between two images and maximizing the similarity between these features. Block matching represents a popular technique and has been widely used for rigid (and affine) and non-rigid image registration. Instead of measuring the global similarity between image features with respect to the global transformation parameters, block matching exploits local similarity measurements of image features and generates a local transformation, from which a global transformation is derived [9].

In block matching-based rigid registration algorithms, the basic concept is to divide the images into blocks and to find the block-wise correspondences. The  $i^{\text{th}}$  subimage or block  $B_m^i(x)$  in the moving image  $I_m(x)$  is moved within a search window and the similarity between block  $B_m^i(x)$  and the block in the fixed image  $I_f(x)$  with coincident positions as  $B_m^i(x)$  is measured, i.e., using sum of absolute differences, cross correlation or mutual information. The block  $\hat{B}_f^i(x)$  that best matches  $B_m^i(x)$  is determined under the matching criterion, resulting in a correspondence between the centre of  $B_m^i(x)$  and the centre of  $\hat{B}_f^i(x)$ . Depending on applications, the computational efficiency of the block-to-block similarity measurements may be improved in a few ways, i.e., subsampling the search window and features in the block for similarity measurements. To facilitate robust estimation of the global transformation matrix  $T$ , outlier correspondences (bad block match) were removed and the remainder were used for a least trimmed squared regression. The correspondences with low regression errors (top 50%) were used to re-estimate the global transformation  $T$  and this process was iterated until convergence.

### 2.2 Cine-MCLE Deformable Registration Using Dual Optimization

From the perspective of energy minimization, deformable registration aims to estimate plausible deformation field  $\phi(x)$  to align two images or to maximize the similarity between a fixed image  $I_f(x)$  and a moving image  $I_m(x)$ ,  $x \in \Omega$ . In cardiac cine and MCLE images, we noticed that the two images are not directly comparable because of different contrast mechanisms [4]. Here we employed the self similarity context (*SSC*) [7] instead of the original image signal intensities for robust similarity measurements of cine and MCLE images. For  $\forall x \in \Omega$ ,  $SSC(x)$  defines an eight-element vector each measuring the exponent of the negative absolute differences of image signal intensities between  $x$  and its eight-neighbour. Therefore, the similarity between  $I_f(x)$  and  $I_m(x)$  can be measured by computing the sum of absolute differences between  $SSC_f(x)$  and  $SSC_m(x)$  under the deformation field  $\phi(x)$ . In addition, the desired “plausible” deformation field was constrained by regularizing the smoothness of  $\phi(x)$  using total

variation, i.e.,  $\int_{\Omega} |\nabla \phi(x)| dx$ . To this end, the deformable registration problem can be formulated by minimizing the energy function  $E(\phi)$  (subject to some given deformation  $\Phi(x)$  if there is) as follows:

$$E(\phi) = \int_{\Omega} \left| SSC_f(x) - SSC_m(x + \Phi + \phi) \right| dx + \alpha \sum_{d=1}^3 \int_{\Omega} |\nabla(\Phi_d + \phi_d)| dx, \quad (1)$$

where the first term measures the similarity between  $I_f(x)$  and  $I_m(x)$  using the respective  $SSC$  under the deformation field  $\phi(x)$  (with given  $\Phi(x)$  if there is), and the second term evaluates the smoothness of the deformation field.

Direct minimization of  $E(\phi)$  (1) is challenging because of the nonlinearity and nonsmoothness of the energy function. Here we employed optical flow technique [8] to decompose the nonlinear similarity measurement term following the fact that  $f(x+t) \approx f(x) + \nabla f(x) \cdot t$ , where  $t$  is the small displacement field between  $f(x)$  and  $f(x+t)$ , and can be obtained by estimating a series of incremental deformation field  $t'(x)$ , i.e.,  $t(x) = \sum_i t'_i(x)$  [6]. In addition, the nonsmooth absolute function terms can be smoothed by introducing additional function, i.e.,  $|g(x)| = \max_{|h(x)| \leq 1} h(x) \cdot g(x)$ . Furthermore, the total variation function can be formulated as  $\int |\nabla q(x)| dx = \max_{|p(x)| \leq 1} \int \text{div} p(x) q(x) dx$  (see [5,6] for detailed analyses). Therefore, we can equivalently rewrite the complicated minimization problem Eq. (1) as follows:

$$\begin{aligned} \max_{|p| \leq 1, |q| \leq \alpha} \min_{\phi} E(\phi; p, q) &:= \int_{\Omega} (p \cdot S_0 + \sum_{d=1}^3 \Phi_d \cdot \text{div} q_d) dx \\ &+ \sum_{d=1}^3 \int_{\Omega} \phi_d \cdot (\text{div} q_d - p \cdot \partial_d S) dx, \end{aligned} \quad (2)$$

where  $S_0 = SSC_f(x) - SSC_m(x + \Phi)$  and  $S = SSC_m(x + \Phi)$ . Clearly, minimization of Eq. (2) over free variable  $\phi_d(x)$  requires vanishing of  $(\text{div} q_d - p \cdot \partial_d S)$ , i.e.,  $(\text{div} q_d - p \cdot \partial_d S) = 0, d \in \{1, 2, 3\}$ . Alternatively, the deformation field  $\phi_d(x)$  just acted as the multiplier function of the respective constraints  $(\text{div} q_d - p \cdot \partial_d S) = 0, d \in \{1, 2, 3\}$ , on top of the maximization component. Therefore, we developed an augmented Lagrangian algorithm based on convex optimization theories [1] to derive the optimal  $\phi_d(x)$  as follows:

$$\max_{|p| \leq 1, |q| \leq \alpha} \min_{\phi} E(\phi; p, q) - \frac{c}{2} \sum_{d=1}^3 \|\text{div} q_d - p \cdot \partial_d S\|^2, \quad (3)$$

where  $c > 0$  is a scale.

Clearly, the dual relationship between Eqs. (2) and (1) indicates that optimization of the convex problem Eq. (2) solves the original registration problem Eq. (1) equivalently but demonstrated greater simplicity in numerics than the original non-linear non-convex formulation (1). In addition, the point-wise iterative implementation of the registration algorithm Eq. (3) (see [6] for the details) leads to high performance parallel implementation on a GPU for speed-up.

### 3 Experiments and Results

#### 3.1 Animal Preparation and MRI Acquisition

Myocardial infarction was generated in 10 pigs (weighing 20–25 kg) by occluding either the left anterior descending artery (LAD) or the left circumflex (LCX) artery. We inflated a balloon catheter in the LAD or LCX for  $\sim 90$  min followed by reperfusion to create heterogeneous infarcts as previous described [10]. The animal study was approved by our institution and the animals were allowed to heal for  $\sim 5$  weeks prior to MR imaging.

MRI was performed at 1.5 T with a GE Signa Excite Scanner. Animals were sedated and the respiration was controlled using a mechanical ventilator. For cine MRI, 2D short-axis slices were acquired using a conventional segmented steady state pulse sequence (SSFP, bandwidth = 125 KHz, number of phases = 20, views per segment = 16, TR/TE/flip angle = 3.7 ms/1.6 ms/45°, field of view =  $23 \times 23$  cm<sup>2</sup>, image matrix =  $256 \times 256$ , NEX = 1, number of slices = 9–18, slice thickness = 5 mm). MCLE images were obtained  $\sim 15$  min after a bolus injection of 0.2 mmol/kg Gd-DPTA (Gd-DPTA Magnevist; Berlex Inc., Wayne, NJ, USA). 2D short-axis images were acquired using an inversion recovery-prepared b-SSFP sequence at different inversion times ranging from 175 to 250 ms (bandwidth = 125 KHz, number of phases = 20, views per segment = 16, TR/TE/flip angle = 5.5 ms/1.9 ms/45°, field of view =  $25.6 \times 25.6$  cm<sup>2</sup>, image matrix =  $256 \times 256$ , slice thickness = 5 mm).

#### 3.2 Algorithm Implementation

MCLE scar heterogeneity was segmented slice-by-slice using a fuzzy-logic clustering approach [3]. For each dataset, one out of the 6–8 images at diastolic phases with minimal cardiac motion was extracted for each slice and the extracted phases for all the slices were stacked into a 3D MCLE image  $I_m(x)$ . Similarly, 1 out of the 20 phases of each cine slice that matches the shape of the heart in MCLE was selected and all the selected phases were stacked into a 3D cine image  $I_f(x)$ . Prior to algorithm registration, 3D cine and MCLE images were interpolated to isotropic voxel size of respective in-plane voxel width ( $\sim 0.9$  mm for cine and  $\sim 1$  mm for MCLE). Both the rigid and deformable registrations were implemented in a coarse-to-fine manner (3 levels, scaling factors =  $\{4, 2, 1\}$ ), whereby large displacements field was estimated in lower levels and smaller displacements field in higher levels. The coarse-to-fine implementation provides both registration accuracy and computational efficiency. For the deformable registration, the given (initial) deformation field  $\Phi(x)$  in Eq. (1) at the lowest level (scaling factor = 4) was set to  $\mathbf{0}$  while for the other levels  $\Phi(x)$  was initialized using the final deformation from the preceding levels. The MCLE scar (infarct core  $\cup$  gray zone) were deformed and fused with cine myocardium masks.

### 3.3 Validation

Cine and MCLE image registration accuracy was evaluated by comparing cine and MCLE myocardium masks. In particular, a single observer manually segmented the myocardium in cine slice-by-slice using ITK-SNAP and the segmentation results were approved by an experienced observer with more than 10 years’ experience in cardiac MRI segmentation. MCLE images were segmented slice-by-slice using a fuzzy-logic clustering approach [3]. For each slice, 6–8 images at diastolic phases with minimal cardiac motion were used for exponential fitting to derive a  $T1^*$  and steady-state (SS) signal intensity value for each pixel. The generated  $T1^*$ -SS maps were classified into: infarct core (IC), gray zone (GZ), healthy myocardium (HM) and blood (B). MCLE myocardium masks were obtained by combining the IC, GZ and HM sub-regions. The derived deformation field was used to warp the MCLE myocardium masks. Cine-MCLE registration accuracy was quantified using Dice similarity coefficient ( $DSC$ ) and average symmetric surface distance ( $ASSD$ ) of cine and MCLE manual myocardium masks. Let  $R_c$  and  $R_m$  be the cine and deformed MCLE myocardium mask, respectively.  $DSC$  is calculated as:  $\frac{2(R_c \cap R_m)}{R_c + R_m} \cdot 100\%$ .  $ASSD$  is given as:  $\frac{1}{2} \left\{ \frac{1}{|\partial R_c|} \sum_{p \in \partial R_c} d(p, \partial R_m) + \frac{1}{|\partial R_m|} \sum_{p \in \partial R_m} d(p, \partial R_c) \right\}$ , where  $\sum_{p \in \partial R_c} d(p, \partial R_m)$  represents the summation of the minimal distance  $d$  from the points  $p$  in surface  $\partial R_c$  to surface  $\partial R_m$  and  $|\partial R_c|$  the total number of points in surface  $\partial R_c$ . In addition, we reported the runtime to evaluate the computational efficiency of our approach.

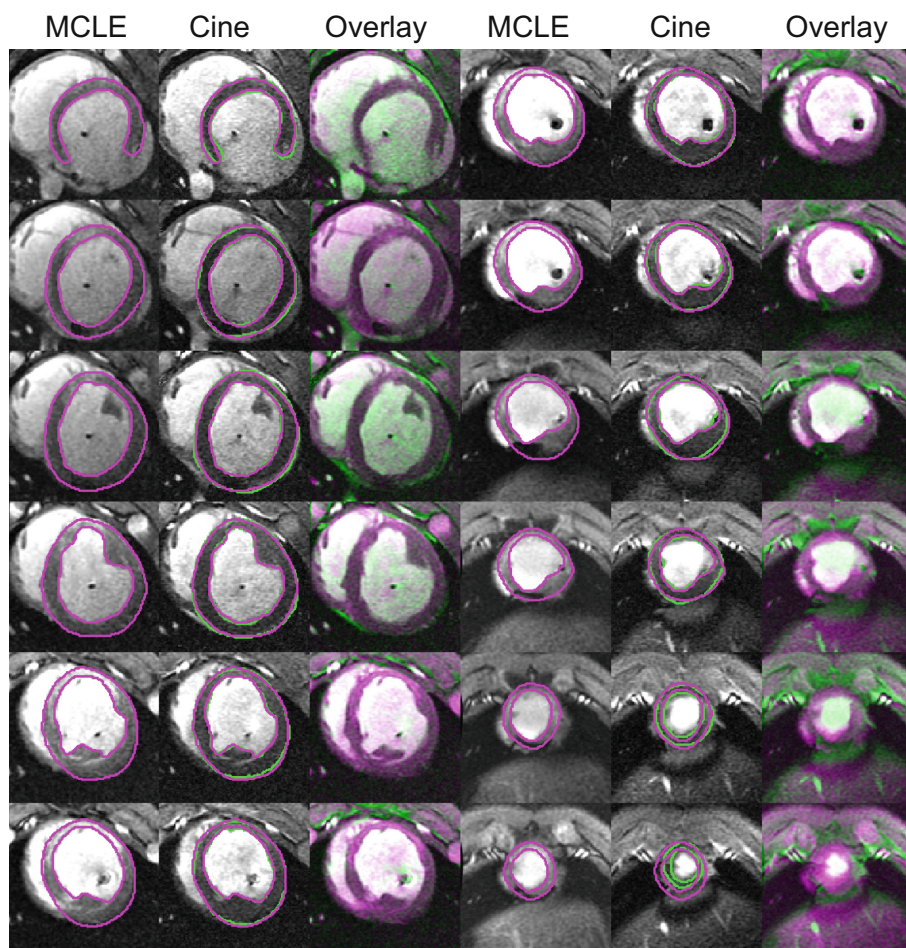
### 3.4 Results

Figure 2 illustrates representative cine-MCLE image registration results. As shown in Table 1, we achieved a mean DSC of  $80.4 \pm 7.8\%$  (range: 62.3%–86.7%) and ASSD of  $1.28 \pm 0.47$  mm (range: 0.82 mm–2.25 mm) by comparing the cine and deformed MCLE myocardium masks in 10 pigs. Figure 3 shows example fused MCLE scar (IC in green and GZ in yellow) and cine myocardium (HM in blue).

All image analysis was performed in 3D space on a Linux Desktop (Ubuntu 14.04, 16G RAM, Inter(R) i7-3770, 3.4 GHz) with a NVIDIA graphics processing unit (GeForce GTX TITAN BLACK). Given pre-segmented MCLE scar geometry, the developed fully automated registration approach required  $\sim 45$  s for the rigid registration,  $\sim 50$  s for the deformable registration refinement, resulting in an overall runtime of  $\sim 1.5$  min for each pig.

**Table 1.** Cine and MCLE registration accuracy measurements. (n = 10)

Pig ID	1	2	3	4	5	6	7	8	9	10	All
DSC (%)	86.7	86.6	76.2	84.8	84.0	84.5	83.5	62.3	72.4	82.6	$80.4 \pm 7.8$
ASSD (mm)	0.82	0.84	1.85	1.27	0.93	1.00	1.26	2.25	1.53	1.05	$1.28 \pm 0.47$



**Fig. 2.** Representative MCLE and cine MRI registration results. **First** and **Fourth** columns: MCLE images and myocardium segmentation (purple contours); **Second** and **Fifth** columns: cine images, cine (green) and deformed MCLE (purple) myocardium contours; **Third** and **Sixth** columns: cine (green) and registered MCLE (purple) image overlay (green or purple shows the differences and gray represents match of the two images.) Basal to apex slices are shown from upper left to lower right. (Color figure online)

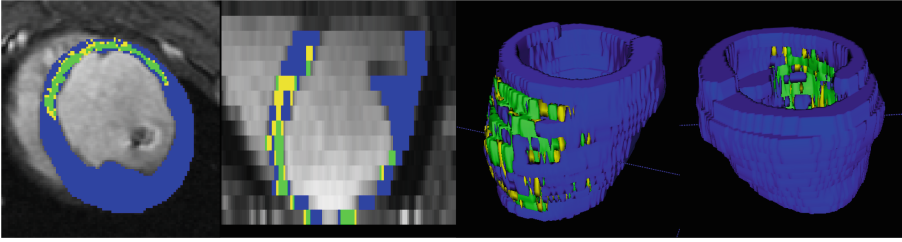


**Fig. 3.** A representative heart model built from cine-MCLE MRI registration and MCLE scar-cine myocardium fusion. Short axis, long axis and 3D view of the heart models are shown from left to right. (Blue: Cine myocardium, Green: MCLE infarct core, Yellow: MCLE gray zone.) (Color figure online)

## 4 Discussion and Conclusions

Cine and MCLE MRI registration provides a way to combine the information from the two imaging methods and holds great promise for improved cardiovascular disease care. In this preclinical study, we developed an approach for automated cine and MCLE image registration and MCLE scar-cine myocardium label fusion. For a group of 10 pigs, we demonstrated cine and MCLE MRI registration accuracy of  $80.4 \pm 7.8\%$  for DSC,  $1.28 \pm 0.47$  mm for ASSD by comparing manual myocardium masks from the two images. The resulting MCLE-scar and cine-myocardium mask fusion provides a way to build high fidelity 3D heart models for image-guided RF ablation therapies and computational modeling of cardiac electro-mechanical function.

Lastly, we acknowledge a number of limitations of this study. MCLE images provide visualization of myocardium but the image quality is generally poor for myocardium segmentation. In parallel, we observed non-smooth MCLE myocardium surfaces due to the displacement between consecutive slices while the myocardium in cine images are smoother. Therefore, we proposed to utilize the smooth myocardium surfaces provided by cine images through MCLE-cine registration. We note that in most cases the myocardium surfaces in cine images are smooth but in some situations the cine myocardium masks present discontinuities. In these situations, the non-smooth myocardium masks may be improved by re-aligning the cine slices prior to MCLE-cine registration, *i.e.*, using the block-matching-based rigid registration approach [9]. Regarding the deformable registration method, our approach required point-wise similarity measurements while other metrics, including global mutual information/cross correlation, also demonstrate promising performance and are widely used in various registration tasks. Unfortunately, these global similarity metrics are not directly amenable to our registration framework further investigations, *i.e.*, relaxing these global measure to point-wise measure are required. Currently, both the cine and MCLE images were acquired in a segment-by-segment and slice-by-slice manner under ECG-gating. However, it is still challenging to ensure the alignment within and between slices due to imperfectness of ECG gating, leading

to jagged myocardium contours along the long-axis direction. Recent developments in fast MR image acquisition methods including compressed sensing and parallel imaging and the combination provide a way for rapid volumetric image acquisition. We think these techniques may mitigate the within and between slice misalignment issue and we are planning to implement fast cine and MCLE volumetric image acquisitions in the future.

## References

1. Bertsekas, D.P.: *Nonlinear Programming*. Athena Scientific, Belmont (1999)
2. Chenoune, Y., et al.: Rigid registration of delayed-enhancement and cine cardiac MR images using 3D normalized mutual information. In: *Computing in Cardiology*, pp. 161–164. IEEE (2010)
3. Detsky, J.S., Paul, G., Dick, A.J., Wright, G.A.: Reproducible classification of infarct heterogeneity using fuzzy clustering on multicontrast delayed enhancement magnetic resonance images. *IEEE Trans. Med. Imaging* **28**(10), 1606–1614 (2009)
4. Detsky, J., Stainsby, J., Vijayaraghavan, R., Graham, J., Dick, A., Wright, G.: Inversion-recovery-prepared SSFP for cardiac-phase-resolved delayed-enhancement MRI. *Magn. Reson. Med.* **58**(2), 365–372 (2007)
5. Guo, F., Capaldi, D.P., Di Cesare, R., Fenster, A., Parraga, G.: Registration pipeline for pulmonary free-breathing 1 H MRI ventilation measurements. In: *Medical Imaging 2017: Biomedical Applications in Molecular, Structural, and Functional Imaging*, vol. 10137, p. 101370A. International Society for Optics and Photonics (2017)
6. Guo, F., et al.: Thoracic CT-MRI coregistration for regional pulmonary structure-function measurements of obstructive lung disease. *Med. Phys.* **44**(5), 1718–1733 (2017)
7. Heinrich, M.P., Jenkinson, M., Papież, B.W., Brady, S.M., Schnabel, J.A.: Towards realtime multimodal fusion for image-guided interventions using self-similarities. In: Mori, K., Sakuma, I., Sato, Y., Barillot, C., Navab, N. (eds.) *MICCAI 2013*. LNCS, vol. 8149, pp. 187–194. Springer, Heidelberg (2013). [https://doi.org/10.1007/978-3-642-40811-3\\_24](https://doi.org/10.1007/978-3-642-40811-3_24)
8. Lucas, B.D., Kanade, T., et al.: An iterative image registration technique with an application to stereo vision (1981)
9. Ourselin, S., Roche, A., Prima, S., Ayache, N.: Block matching: a general framework to improve robustness of rigid registration of medical images. In: Delp, S.L., DiGoia, A.M., Jaramaz, B. (eds.) *MICCAI 2000*. LNCS, vol. 1935, pp. 557–566. Springer, Heidelberg (2000). [https://doi.org/10.1007/978-3-540-40899-4\\_57](https://doi.org/10.1007/978-3-540-40899-4_57)
10. Pop, M., et al.: Quantification of fibrosis in infarcted swine hearts by ex vivo late gadolinium-enhancement and diffusion-weighted MRI methods. *Phys. Med. Biol.* **58**(15), 5009 (2013)
11. Tao, Q., Piers, S.R., Lamb, H.J., van der Geest, R.J.: Automated left ventricle segmentation in late gadolinium-enhanced mri for objective myocardial scar assessment. *J. Magn. Reson. Imaging* **42**(2), 390–399 (2015)
12. Wei, D., Sun, Y., Chai, P., Low, A., Ong, S.H.: Myocardial segmentation of late gadolinium enhanced MR images by propagation of contours from cine MR images. In: Fichtinger, G., Martel, A., Peters, T. (eds.) *MICCAI 2011*. LNCS, vol. 6893, pp. 428–435. Springer, Heidelberg (2011). [https://doi.org/10.1007/978-3-642-23626-6\\_53](https://doi.org/10.1007/978-3-642-23626-6_53)